X. Manipulation of Molecules by Combined Permanent and Induced Dipole Forces

B. Friedrich[a,*]

[a] Fritz-Haber-Institut der Max-Planck-Gesellschaft

Faradayweg 4-6, D-14195 Berlin, Germany

*corresponding email address: bretislav.friedrich@fhi-berlin.mpg.de

ABSTRACT

This chapter describes a versatile technique to control molecular rotation and translation. The technique is based on the combined effect of external electric fields that act concurrently on the molecular permanent and induced dipole moments. This synergistic effect arises for any polar molecule, as only an anisotropic polarizability, along with a permanent dipole moment, is required. This is always available in polar molecules. The effect of the combined fields can be achieved either by superimposing an electrostatic and a far-off resonant optical field (i.e., one that supplies electric field strength but does not cause transitions) that act, respectively, on the molecule's permanent and induced electric dipole, or by making use of a unipolar electromagnetic pulse that seizes the permanent and induced dipole moments simultaneously. If the combined electric fields are homogeneous, only molecular rotation is affected, whereas inhomogeneous fields affect both molecular rotation and translation. As noted in the chapter, the ability to manipulate molecular rotation and translation has wide-ranging applications – in research areas as diverse as reaction dynamics, spectroscopy, higher harmonic generation and molecular

orbital imaging, the focusing and trapping of molecules, as well as quantum simulation and computing.

X.1 Introduction

All molecules possess a handle that can be used to manipulate their rotation and/or translation. This metaphorical handle is the molecular electric dipole moment, either *permanent*, if the molecule is polar, or *induced*, if it is non-polar. Pulling on the handle by an external electric field affects foremost the rotational and/or translational degrees of freedom of the molecule and provides the means for their manipulation.

The ability to manipulate molecular rotation and translation has been crucial to progress in research areas and applications ranging from reaction stereodynamics to orbital imaging to molecular focusing and trapping. Table X.1 provides a partial survey along with key references.

The permanent and induced dipole moments behave differently when acted upon by an external electric field: while the permanent dipole moment becomes *oriented* in the direction of the field (and behaves like a *single-headed arrow*), the induced dipole moment *aligns* along the field (and behaves like a *double-headed arrow*). Hence we speak of *orienting* and *aligning interactions*. These interactions can be combined, resulting in a sui generis compounded behaviour of the dipoles involved. Quite often, even a very weak orienting interaction can convert second-order alignment into a strong first-order orientation.[1,2,3,4,5,6]

47

48 In what follows, we will introduce the Hamiltonian for a molecule subject to orienting,
49 aligning, and combined interactions and discuss the most notable features of the
50 stationary (time-independent) solutions of the corresponding Schrödinger equation.
51 These solutions comprise the *directional* (i.e., oriented and/or aligned) states
52 produced as well as the surfaces of the corresponding eigenenergies spanned by
53 the parameters characterizing the strengths of the orienting and aligning
54 interactions.[7]

55

56 Remarkably, the Schrödinger equation for the combined interaction is *conditionally*
57 *quasi-solvable*, i.e., it possesses some analytic solutions for certain conditions
58 imposed on the orienting and aligning parameters. The rest of the solutions has to be
59 found numerically. We will show that the Schrödinger equation in question is that of
60 the *generalized quantum pendulum* (GQP) and examine the conditions of analytic
61 solvability for the GQP eigenproblem and their relation to the topology of the GQP's
62 eigenenergy surfaces. This examination will reveal a profound connection between
63 the conditions and the topology.[8,9,10]

64

65 The temporal dependence of the external electric field that acts on the molecule is
66 highly consequential for the outcome of the interaction.[2,5,11,12] Clocked by the
67 molecule's rotational period, the temporal dependence may result either in an
68 *adiabatic* (if the field varies slowly with respect to the rotational period) or *non-*
69 *adiabatic* interaction (otherwise). We note that the notion of an adiabatic or non-
70 adiabatic change has its counterpart in molecular dynamics, where it refers to the

compatibility or incompatibility of time scales for the relative motion of the electrons and nuclei in a given polyatomic system.

When the external field is applied as a pulse much shorter than the rotational period of the molecule, we speak of a *delta* pulse and a *sudden* interaction. We will examine the sudden interaction as it arises for a *unipolar* electromagnetic pulse and represent its salient features in terms of *population quilts* and *quantum carpets*. What is perhaps most surprising – and useful – about the non-adiabatic interaction is that it results in field-free orientation and alignment of the molecule that recurs at multiples (also fractional ones) of the rotational period.

A section is dedicated to guiding the reader through examples that are intended to provide a feeling for the numerical values involved.

Applications benefitting from the ability to manipulate molecular rotation/translation	References
Molecular alignment/orientation	Ref.[13,14,15,16,17,18,19,20,21,22]
Deflection, focusing and trapping	Ref.[23,24,25,26,27]
Reaction Stereodynamics	Ref.[28,29,30]
Stark spectroscopy	Ref.[31,32]
Photoelectron angular distributions	Ref.[33,34,35]
Diffraction from within	Ref.[36,37]
High-order harmonic generation and orbital imaging	Ref.[38,39,40,41,42,43]
Quantum simulation and computing	Ref.[44,45,46,47,48,49,50,51,52]
Molecular movies	Ref. [53,54,55]
Molecules embedded in superfluid helium droplets	Ref. [56,57,58,59]

Table X.1: Partial survey of research areas and applications benefitting from the ability to manipulate molecular rotation and/or translation. Apart from seminal work, only the most recent representative references are listed.

X.2 The Hamiltonian of a Linear Polar and Polarizable Molecule Subject to Combined Orienting and Aligning Interactions

For a linear polar and polarizable molecule, cf. Fig. X.1, the Hamiltonian takes the form

$$H = B\mathbf{J}^2 + V_\mu + V_\alpha \qquad (1)$$

where $\mathbf{J}^2$ is the angular momentum squared, $B = \hbar^2/(2I)$, with I the moment of inertia, is the rotational constant,

$$V_\mu = -\mu F_1 \cos\theta \qquad (2)$$

is the permanent-dipole interaction potential, with μ the permanent electric dipole moment along the internuclear axis *r* and θ the polar angle between the permanent dipole and the electric field strength vector of magnitude F_1, and

$$V_\alpha = -\frac{1}{2}\Delta\alpha F_2^2 \cos^2\theta - \frac{1}{2}\alpha_\perp F_2^2 \qquad (3)$$

is the induced-dipole interaction potential, with $\Delta\alpha = \alpha_{||} - \alpha_\perp$ the polarizability anisotropy arising from the polarizability components $\alpha_{||}$ and $\alpha_\perp$ parallel and perpendicular to the intermolecular axis *r*, and θ the polar angle between the induced dipole and the electric field strength vector of magnitude F_2. Note that herein we consider the case when the field vectors are collinear. The electric vector $\mathbf{F}_1$ (of magnitude F_1) is due to an electrostatic field; the electric vector $\mathbf{F}_2$ (of magnitude F_2) can be either due to an electrostatic field (in which case $F_1 = F_2$) or a laser field of intensity *S*, in which case $F_2 = [2S/(c\varepsilon_0)]^{1/2}$, with *c* the speed of light in vacuum and ε_0 the vacuum permittivity. The fields F_1 and F_2 can be also due to a unipolar pulse, in which case $F_1 = F_2$ as well.

The Hamiltonian of Eq. (1) can be conveniently recast in dimensionless form by dividing through the rotational constant,

$$H/B \equiv \mathcal{H} = \mathbf{J}^2 - \eta\cos\theta - \zeta\cos^2\theta \qquad (4)$$

with the dimensionless parameters

$$\eta = \frac{\mu F_1}{B} \qquad (5)$$

and

$$\zeta = \frac{\Delta\alpha F_2^2}{2B} \qquad (6)$$

termed the *orienting* and *aligning parameters*. They express the strengths of either interaction independent of the properties (dipole moments, polarizabilities, rotational constants) of any particular molecule. In Hamiltonian (4) we omitted the constant second term arising from the induced-dipole potential (3), as its only effect is a uniform shift of the Hamiltonian's energy levels.

[Insert Figure X.1 here]

Molecule	B [cm^{-1}]	μ [Debye]	$\Delta\alpha$ [Å^3]	t_r [ps]	Reference
HD	45.644	5x10^{-4}	0.305	0.037	Ref.[60]
DCl	5.445	1.18	0.74	0.306	Ref.[61]
HI	6.551	0.43	0.45	0.255	Ref.[62,63,64]
DI	3.253	0.38	1.69	0.513	Ref.[61]
NO	1.703	0.16	2.8	0.980	Ref.[61]
CO(X)	1.931	0.10	1.0	0.864	Ref.[61]
CO(a)	1.681	1.37	1.5	0.992	Ref.[61]
HCN	1.482	3.00	2.0	1.126	Ref.[61]
ICN	0.1075	3.72	7.0	15.52	Ref.[61]
CsF	0.1843	7.97	3.0	9.051	Ref.[61]
LiNa	0.38	0.566	24.7	4.390	Ref.[65,66]
LiCs	0.188	5.52	49.5	8.873	Ref.[65,66]
NaK	0.091	2.76	39.5	18,33	Ref.[65,66]
KCs	0.033	1.92	64.6	50.55	Ref.[65,66]
RbCs	0.016	1.27	72.8	104.3	Ref.[65,66]
OCS	0.2039	0.709	4.1	8.181	Ref.[61]
KRb	0.032	0.76	54.1	52.13	Ref.[65,66]
HCCCl	0.1067	0.44	4.1	15.63	Ref.[61]
HCCCN	0.1516	3.60	6.0	11.00	Ref.[61]
HArCCH	0.118	5.25	15.31	14.14	Ref.[67]
HXeCCH	0.081	3.41	11.81	20.60	Ref.[67]
HXeI	0.027	6.4	3.4	61.78	Ref.[62,63,64]
Benzene-Ar	0.039	0.12	-6.1	42.77	Ref.[68]

Table X.2: Rotational constants B, electric dipole moments μ and polarizability anisotropies $\Delta\alpha$ and rotational periods t_r of a sampling of molecules. Note that $\eta = 1.68\times10^{-2}\ F_1$ [kV/cm] [Debye]/B [cm^{-1}], $\zeta = 2.79\times10^{-8}\ F_2^2$ [kV^2/cm^2] $\Delta\alpha$ [Å^3]/B [cm^{-1}] = $1.05\times10^{-11}\ S$ [W/cm^2] $\Delta\alpha$ [Å^3]/B [cm^{-1}], and t_r [ps] = $1.6682/B$ [cm^{-1}]. We note that an electrostatic field F_1 = 100 kV/cm acting on a permanent electric dipole moment of 1 Debye corresponds to an energy of 4.8 cal/mol; an optical field $S = 10^{10}$ W/cm^2

(corresponding to F_2 = 1941 kV/cm) acting on an induced dipole arising from a polarizability of 1 Å^3 corresponds to 3 cal/mol. A wavenumber (1 cm^{-1}) corresponds to 2.9 cal/mol.

The Hamiltonian of Eq. (4) is recognized as that of the Generalized Quantum Pendulum (GQP).[9,10] Hence a polar and polarizable molecule is one of the GQP's realizations.

Table X.2 provides a list of molecular properties for a selection of linear molecules, along with the conversion factors that are needed for evaluating the orienting and aligning parameters for given field strengths. Note that $\Delta\alpha > 0$ for linear molecules, but can be negative for symmetric or asymmetric tops. In order to achieve sizable values of the aligning parameter (say, $\zeta > 10$), the requisite field strength F_2 has to be on the order of 10^4 kV/cm for most of the molecules listed, which can only be provided by a pulsed electromagnetic field (S =10^{12} kW/cm^2 corresponds to 1.941×10^4 kV/cm). Sizable values of the orienting parameter (say, $\eta \approx 10$) can often be achieved by an electrostatic field F_1 on the order of 100 kV/cm.

X.2. The Schrödinger Equation for Molecules Subject to Combined Orienting and Aligning Interactions

The time-independent Schrödinger equation pertaining to Hamiltonian (4)

$$\mathcal{H}\left|J,|M|;\eta,\zeta\right\rangle = E_{J,|M|}(\eta,\zeta)\left|J,|M|;\eta,\zeta\right\rangle \qquad (7)$$

reduces at vanishing orienting and aligning interactions to that for a free rotor

$$\mathbf{J}^2 \left| J,|M| \right\rangle = E_{J,|M|} \left| J,|M| \right\rangle \qquad (8)$$

where the respective wavefunctions are related by $\left| J,|M|;\eta=0,\zeta=0 \right\rangle \rightarrow \left| J,|M| \right\rangle$. Hence the states created by the combined orienting and aligning interactions can be labelled by the angular momentum quantum numbers *J* and *M* of the field-free rotor state from which they arose upon switching on the interactions. Since the sense of rotation makes no difference, only |*M*|, the magnitude of *M*, matters.

Likewise, the eigenenergies, measured in terms of the rotational constant *B*, are related by $E_{J,|M|}(\eta=0,\zeta=0) \rightarrow E_{J,|M|} = J(J+1)$. The field-free states $\left| J,|M| \right\rangle$ have a definite parity, given by $p = (-1)^J$. We note that parity is a symmetry property of the wavefunction (of a given state) that indicates whether the wavefunction changes its sign upon inversion of the coordinates (in which case $p = -1$) or not ($p = +1$). States of *definite* parity, i.e., states with either $p = +1$ or $p = -1$, cannot be oriented. We'll see below that in order to orient a molecule, we have to put in into a state whose parity is *indefinite* (i.e., neither +1 nor –1). We speak also of a state of mixed parity, as it arises by mixing (linear superposition) of several states with opposite parities.

The wavefunction due to the combined orienting and aligning interactions

$$\left| J,|M|;\eta,\xi \right\rangle = \sum_J c_J(\mu,\xi) \left| J,|M| \right\rangle \qquad (9)$$

is a *hybrid* (coherent linear superposition) of the field-free wavefunctions $|J,|M|\rangle$ for a fixed value of the good quantum number *M* and for a range of *J*'s. The expansion (or hybridization) coefficients $c_J(\mu,\zeta)$ depend on the orienting and aligning parameters and, generally, have to be found numerically. Note that the wavefunction of Eq. (9) depends on the polar coordinates θ and ϕ (via the field free rotor basis wavefunctions) and could be alternatively written as $\Psi_{|J,|M|\rangle}(\theta,\phi;\eta,\zeta)$. Its modulus, $|\Psi_{|J,|M|\rangle}(\theta,\phi;\eta,\zeta)|^2$, gives the probability density of the polar and azimuthal angles θ and ϕ of the molecule in that state.

[Insert Figure X.2 here]

A key feature of the orienting interaction $(\propto \eta\cos\theta)$ is that it couples field-free rotational states whose *J*'s differ by ±1, whereas the aligning interaction $(\propto \zeta\cos^2\theta)$ couples free-rotor states with *J*'s that are either the same or differ by ±2. As a result, the orienting interaction creates states of mixed (indefinite) parity while the aligning interaction preserves parity. Thus, as long as $\eta \neq 0$, wavefunction (9) is of indefinite/mixed parity as well. As noted above, this is a precondition for orientation: only states of indefinite parity can be oriented.

The number of *J*'s involved in a given hybrid wavefunction is infinite in principle but, for the ground state, on the order of the orienting/aligning parameters in practice, i.e., if the eigenproperties are to be evaluated with an accuracy sufficient for most applications. Generally, the higher the initial *J* of a state, the fewer rotational basis states are drawn into its hybrid wavefunction at a given value of the interaction

parameter (either η or ζ). This is because of the $J(J+1)$ rotational energy ladder and hence the increasing separation of the rotational basis states that make up the hybrid.

That there's no hybridization of the angular momentum projection quantum number M in collinear orienting and aligning fields follows from the cylindrical symmetry of the problem (there is just a single axis of cylindrical symmetry given by the common direction of $\mathbf{F}_1$ and $\mathbf{F}_2$). Once this symmetry is broken (i.e., if the fields $\mathbf{F}_1$ and F_2 are not collinear), M ceases to be a good quantum number and states with different M's are hybridized as well.

X.2.1 Eigenenergy Surfaces and their Intersections for Molecules Subject to Combined Orienting and Aligning Interactions

All states bound by the aligning interaction occur as doublets split by tunnelling through the equatorial barrier of the V_α potential, cf. Fig. X.2. The members of any tunnelling doublet have same $|M|$ but opposite parities. The tunnelling splitting, ΔE, scales as

$$\Delta E(\zeta) \propto \exp(-\zeta^{1/2}) \qquad (11)$$

and so the members of any given tunnelling doublet can be drawn arbitrarily close to one another by boosting ζ. Once the parity-mixing orienting potential V_μ is superimposed, see Fig. X.3, the symmetry of the two equivalent minima of V_α at $\theta =$

228 0^o and 180^o is broken and the tunnelling levels repel each other, at a given ζ,

229 proportionately to η

230 $$\Delta E(\eta,\zeta) \propto \eta \qquad (12)$$

231 [Insert Figure X.3 here]

232 Fig. X.4 shows the eigenenergies as a function of the orienting parameter η for a

233 fixed sizable value of the aligning parameter, ζ= 58. One can see that at η = 0

234 (when the orienting interaction is switched off), this value of ζ is sufficiently high to

235 make the two lowest tunneling doublets depicted (0,0 and 1,0 as well as 3,0 and 2,0)

236 quasi-degenerate, whereas the uppermost doublet shown (4,0 and 5,0) exhibits a

237 marked splitting, as its members are bound only by the upper reaches of the V_α

238 potential. Given that the tunneling splitting at fixed ζ scales linearly with η, the upper

239 member of the lower tunneling doublet is bound to meet the lower member of the

240 upper tunneling doublet at some value of η. This results in a pattern of intersections

241 – all of which are avoided. This is because the intersecting levels originate in the

242 doublet states of opposite parity and, therefore, undergo coupling by the parity-

243 mixing orienting interaction V_μ.

244

245 What are the loci of the avoided intersections? Remarkably, these can be

246 determined analytically, with the result

247 $$\zeta = \frac{1}{4k^2}\eta^2 \qquad k = 1,2,3... \qquad (13)$$

This simple parabolic formula describes how orienting and aligning parameters are connected with one another at all the avoided intersections that arise for the GQP eigenproblem. As we can see, the integer *k*, termed the *topological index*, labels the intersections. And, in fact it does much more than that, as we'll see below.

[Insert Figure X.4 here]

X.2.2 Directional States of Molecules Subject to Combined Orienting and Aligning Interactions

The states that are created by the orienting or aligning interactions alone or by their combination are directional, i.e., they exhibit orientation or alignment or both. A measure of the directionality of the states are the expectation values of the $\cos\theta$ or the $\cos^2\theta$ operators, i.e.,

$$\left\langle \cos\theta \right\rangle = \left\langle J,|M|;\eta,\zeta \left| \cos\theta \right| J,|M|;\eta,\zeta \right\rangle \tag{14}$$

and

$$\left\langle \cos^2\theta \right\rangle = \left\langle J,|M|;\eta,\zeta \left| \cos^2\theta \right| J,|M|;\eta,\zeta \right\rangle \tag{15}$$

which are termed, respectively, the *orientation* and *alignment cosines*. These can be evaluated for any given state either directly from the state's wavefunction, as ordained by Eqs. (14) and (15), or from the field dependence of the state's eigenenergy via the Hellmann-Feynman theorem,

$$\left\langle \cos\theta \right\rangle = -\frac{\partial E_{J,|M|}(\eta,\zeta)}{\partial \eta} \tag{16}$$

$$\left\langle \cos^2\theta \right\rangle = -\frac{\partial E_{J,|M|}(\eta,\zeta)}{\partial \zeta} \qquad (17)$$

The latter method is particularly instructive, as it connects directionality of a molecule with its behavior in a field gradient. For a purely orienting interaction, the orientation cosine of a given state can be negative or positive, depending on whether the state's eigenenergy increases or decreases with the increasing orienting parameter, i.e., whether the state is *low-* or *high-field seeking* (a molecule in a low-field seeking state subject to an inhomogeneous field seeks a region of minimum field strength where its energy is minimal; a molecule in a high-field seeking state seeks a region of maximum field strength where *its* energy is minimal). Therefore, in a low-field seeking state, the molecule is oriented oppositely with respect to the orienting field – it exhibits the *wrong-way orientation*. In a high-field seeking state, the molecule is *right-way oriented*, i.e., in the direction of the orienting field. In dynamical terms, this means that the dipole spends most of its time pointing either against or in the direction of the orienting field vector. See also Textbox 3 in Chapter 1.

In contrast, all states created by the aligning interaction are high-field seeking, since the aligning interaction is purely attractive. However, a given state can still be *right-* or *wrong-way aligned*, depending on whether the induced dipole is aligned along or perpendicular to the aligning field vector.

The combined orienting and aligning interactions produce intriguing directional effects. Apart from creating strong orientation for essentially any polar molecule, the combined fields lead to a sui generis dependence of the orientation on the strength

of the fields. The salient features of the directional states and their field dependence are exemplified by the behaviour of the 0,0-1,0 tunnelling doublet in Fig. X.5 and of the 1,1-2,1 tunnelling doublet in Fig. X.6.

At aligning interactions strong enough to make the doublets quasi-degenerate, even a tiny orienting interaction converts alignment into strong orientation. This is illustrated by the polar plots of the squares of the wavefuntions at η = 0.1 and 1 for ζ = 10 (full curves) and at η = 10 for ζ = 50 (dashed curves). In either case, the lower member of the tunnelling doublet is high-field seeking (shifts down in energy when the orienting interaction is turned on) while the upper member is low-field seeking (shifts up). As a result, the members of the tunnelling doublets are oppositely oriented with respect to one another – with the lower member right-way oriented and the upper member wrong-way oriented. However, at a sufficiently strong orienting interaction, i.e., at η = 10 for ζ = 10 and η = 20 for ζ = 50 in our examples, the orienting field prevails and both members of the tunnelling doublets become right-way oriented. Also shown in Figs. X.5 and X.6 are the pertinent values of the orientation and alignment cosines.

In the combined fields, the wrong-way orientation effect arises at small orienting interactions for all states that are “slated” to become the upper members of the tunneling doublets. Such states have J–$|M|$ odd. The states “slated” to become the lower members of the tunnelling doublets, with J–$|M|$ even, are all high-field seeking and, therefore, right-way oriented at all non-zero values of η and ζ.

[Insert Figure X.5 here]

This behavior contrasts with that for a purely orienting interaction: for $\eta > 0$ and $\zeta = 0$, states with the tilt angle

$$\gamma = \arccos \frac{|M|}{[J(J+1)]^{1/2}} \qquad (18)$$

of the angular momentum with respect to the field vector exhibit wrong-way orientation at small values of η for $\gamma > 3^{-1/2}$ and right-way orientation otherwise. This behavior is connected with the slow-down/speed-up of the pinwheeling dipole when it points in the direction opposite to/of the field and arises at values of η that are too small for the V_μ potential to bind the dipole (i.e., confine it to an angular range less than 360^o and thus make the state *pendular*).

[Insert Figure X.6 here]

X.3 Conditional Quasi-Solvability of the Schrödinger Equation for a Molecule Subject to Orienting and Aligning Interactions

Analytic solutions are the gems of physics – beautiful and rare. To our delight, it turned out that the Schrödinger equation for a molecule subject to orienting and aligning interactions – which, as noted above, amounts to the generalized quantum pendulum eigenproblem – is *conditionally quasi-solvable*. This means that analytic solutions can be obtained only under certain conditions imposed on the parameters that characterize a given eigenproblem – in the case of the GQP the orienting and

aligning parameters. And that the analytic solutions can be obtained only for some of the eigenstates, i.e., not for the whole spectrum of the Hamiltonian (by analytic solutions we mean solutions that are expressed in terms of elementary functions).

In seeking the analytic solutions, we made use of three techniques: (1) ad hoc[69]; (2) supersymmetric quantum mechanics[9]; (3) the quantum Hamilton-Jacobi theory[10]. While guessing a viable *Ansatz* is the basis of (1) and (2), (3) offers a systematic way of generating analytic solutions but requires an educated guess concerning the coordinates in which to express them. This task is less ad hoc than (1) and (2) and therefore easier to fulfil.

So far, we have been able to find a cornucopia of analytic solutions – altogether 40 normalizable ones, to be exact, cf. Ref[10]. However, there are reasons to believe that we could find infinitely many solutions to the GQP eigenproblem, although the analytic solutions would not be available for all states: the rest would have still to be handled numerically.

The conditions of quasi-analytic solvability imposed on the η and ζ parameters that we found came out the same for all three techniques. Lo and behold, these conditions coincide with equation (13) for the loci of the avoided intersections of the problem's eigenenergy surfaces!

This close connection is illustrated in Fig. X.7, which pertains to $M = 0$ as an example. In this case, there is only one analytic solution, pertaining to the topological index $k = 1$. Its eigenenergy, marked in red, appears at the intersection of the eigenenergy of the ground state 0,0 (which is the only stretched state for $M = 0$) with the "glass" parabolic surface (which runs through the intersections) at $k = 1$. Note that along the red curve on the 0,0 surface, the eigenvalue of the infinite-dimensional Hamiltonian matrix reduces to a quadratic function of the interaction parameter ζ. We note that, in general, the number of avoided intersections that a given eigenenergy surface partakes in is given by its label J. There are no analytic solutions either for $k = 0$ or $k \to \infty$, i.e., nor for the purely orienting nor for the purely aligning interaction. And there are, of course, no analytic solutions for noninteger values of k either, cf. Eq. (13).

[Insert Figure X.7 here]

We note that the analytic solutions found can be used to evaluate, in closed form, the characteristics of the strongly oriented and aligned molecular states. This may be of practical significance in that one could reverse-engineer the eigenproblem and find the values of the parameters required for creating quantum states with preordained characteristics. Orientation and alignment cosines in analytic form for stretched states (i.e., states with $J = |M|$) that fulfil the analytic solvability condition (13) are given in Ref.[70] Let us mention, as an example, the orientation cosine of the $|J = 0, M = 0; \eta, \zeta\rangle$ ground state featured in Fig. X.7: It is $\langle \cos\theta \rangle = \coth(2\beta) - 1/(2\beta)$, with $\beta = \eta/[2|M| + 1] = \sqrt{\zeta}$.

Analytic solutions can also be used as benchmarks to check numerical calculations or as *Ansatz* for treatments based on perturbation theory.

X.4 Dynamics of Molecules Subject to Combined orienting and Aligning Interactions

So far, we have been dealing with the eigenstates and eigenenergies of Hamiltonian (4), which obtain as the solutions to the time-independent Schrödinger equation (7) or, equivalently, as the stationary solutions to the time-dependent Schrödinger equation

$$i\frac{\partial}{\partial t}\left|J,|M|;\eta,\zeta;\tau\right\rangle = \mathcal{H}\left|J,|M|;\eta,\zeta;\tau\right\rangle \qquad (19)$$

where $\left|J,|M|;\eta,\zeta;\tau\right\rangle$ is the time-dependent wavefunction, which could also be written as $\Psi_{\left|J,|M|\right\rangle}(\theta,\phi;\eta,\zeta;\tau)$, cf. the comment following Eq. (9). Apart from the dimensionless Hamiltonian $\mathcal{H}$, Eq. (19) makes use of dimensionless time $\tau = Bt/\hbar$, which measures time t in terms of the rotational period $t_r = \pi\hbar/B$. Hence we can say that the time dependence of Schrödinger equation (19) is clocked by the rotational period of the molecule. We note that if time t runs for the duration of a rotational period, $t = t_r$, the reduced time $\tau = \pi$.

Eq. (19) yields stationary solutions if the interactions encapsulated in Hamiltonian $\mathcal{H}$ are turned on and off slowly with respect to the rotational period, i.e., over a time $\tau =$

$\tau_0 > \pi$. In that case, we speak of an *adiabatic interaction*, in the course of which the effect of the orienting and aligning fields is the same as if the fields were static at any given time τ. Once the interaction is over, the molecule continues rotating as if no interaction had taken place, quite independent of how dramatic the effects (in terms of orientation and alignment) may have been when the fields were on.

In the opposite, non-adiabatic limit, i.e., when the interactions take place over a time τ_0 much shorter than the rotational period $\tau = \tau_0 << 1$, a rotational wavepacket is formed

$$\left|J_0,|M_0|;\eta,\zeta;\tau\right\rangle = \sum_{J=J_0}^{\infty} c^J_{J_0,|M_0|}(\eta,\xi)\exp[-iJ(J+1)\tau]\left|J,|M_0|\right\rangle \qquad (20)$$

that undergoes revivals whose timing is determined by the rephasing of the field-free rotor states $\left|J,|M_0|\right\rangle$. The contributions of the $\left|J,|M_0|\right\rangle$ states to the wavepacket are determined, in the interaction representation used herein[11], by the time-independent hybridization coefficients $c^J_{J_0,|M_0|}(\eta,\xi)$; these do depend, however, on the orienting and aligning parameters η and ζ. $\left|J_0,|M_0|\right\rangle$ is the initial state the molecule was in before the non-adiabatic interaction struck.

The strengths of the orienting and aligning interactions are conveniently characterized by dimensionless quantities termed *kick strengths*,

$$P_\eta = \int_0^{\tau_0} \eta(\tau)d\tau \qquad \text{and} \qquad P_\varsigma = \int_0^{\tau_0} \varsigma(\tau)d\tau \qquad (21)$$

421 which allow comparing the dynamics that arises from kicks of different shapes,
422 lengths, and strengths and that last over a time $0 \le \tau \le \tau_0$.

423 [Insert Figure X.8 here]

424 Recently developed semiconductor technologies have made it possible to produce
425 electromagnetic pulses that consist of only a *single oscillation cycle* of an
426 electromagnetic wave. Moreover, the distribution of the electric field strength over
427 the cycle can have a bias that favors the oscillation amplitude in one direction over
428 the other. Fig. X.8 shows such a "*unipolar*" pulse. Apart from its larger amplitude in
429 the positive direction than in the negative one, the field F (= F_1 = F_2) has also a
430 different temporal dependence over the time intervals $\tau_+ << \tau_-$: while the positive
431 branch varies quickly (on the order of a picosecond), leading to a non-adiabatic
432 interaction (given that the rotational periods even of small molecules, with the
433 exception of diatomic hydrides, are at least about ten-fold, cf. Table X.1), the
434 negative branch varies slowly, giving rise to an adiabatic interaction. As a result,
435 once the "unipolar" pulse has passed, only the upper branch leaves behind a
436 recurring rotational wavepacket, while the lower branch leaves the molecule in the
437 same stationary state in which it had been before the arrival of the unipolar pulse.
438 The positive branch can be well modelled by a Gaussian which, for small $\tau_+ = \tau_0$ can,
439 in turn, be modelled by a delta function.

440

441 For a *delta-kick* (i.e., a kick due to a delta function), the time dependent Schrödinger
442 equation (19) has analytic solutions (that have nothing to do with the conditional
443 quasi-solvability of the GQP eigenproblem). These solutions correspond to a
444 simultaneous seizure of both the permanent (if available) and induced dipole

moments by the unipolar pulse – and consist of solutions for an aligning delta kick (which are proportional to confluent hypergeometric functions) and an orienting kick (which are proportional to spherical Bessel functions, a special case of the hypergeometric functions). These solutions allow to evaluate all the dynamical observables in analytic form – thereby offering an unrivalled insight into the kicked-rotor dynamics.

[Insert Figure X.9 here]

X.4.1 Population Analysis: Population Quilts

A telling indicator of the effects of the kicks are the resulting post-pulse populations of the rotational states that make up the rotational wavepacket of Eq. (20). These are determined by the squares of the hybridization coefficients, $[c^{J}_{J_0,|M_0|}(\eta,\xi)]^2$. Fig. X.9 shows a representation, in the form of a "*population quilt*," of the post-pulse populations of the rotational states excited by delta-kicks of varying strength. The initial state of the molecule is its ground state, with J_0=0 and M_0=0. The effect of the orienting interaction are manifest near the ordinate: with increasing kick strength, the quantum number J of the most populated level increases in steps of 1, in keeping with the selection rule $\Delta J = \pm 1$ for the orienting interaction. On the other hand, near the abscissa, the quantum number of the most populated level increases in steps of 2, in keeping with the selection rule $\Delta J = \pm 2$ for the aligning interaction. However, the populations along the diagonal – excited by both the orienting and aligning interactions – behave in an unexpected way: the most populated states are those with J = 0 and 1 and they just alternate over the range of kick strengths investigated.

Thus the combined permanent and induced dipole forces give rise to a sui generis population dynamics.

X.4.2 Space-time Portraits: Quantum Carpets

The square of the wavefunction, Eq. (20), gives the probability density of the polar angle θ between the axis *r* of the molecule and the common direction of the orienting and aligning fields as a function of time τ. A contour plot of the probability density as a function of τ is customarily termed a *quantum carpet*. Its rich patterns reveal details about the dynamics of the molecule's interaction with the fields.

Perhaps the most striking pattern that one can glean from the quantum carpets, see Figs. X.10 and X.11, is that of the revivals of the rotational wavepacket: the initial and final state of the wavepacket recurs upon an integer multiple of the revival time, $\tau_{rev} = \pi$. However, due to the presence of even and odd *J*'s in the wavepacket, also fractional revivals (revivals at integer fractions of τ_{rev}) are present.

[Insert Figure X.10 here]

For the purely orienting interaction, see panels (a) in Figs. X.10 and X.11, the carpets exhibit inversion symmetry with respect to the point $\theta = \tau = \pi/2$. This has its origin in the parity transformation properties of the field-free rotor states. The complex pattern due to the purely aligning interaction, see panels (b) of Figs. X.10 and X.11, is comprised of nearly isotropic islands, which are mimicking the isotropic distribution of the initial $|0,0\rangle$ state. These become increasingly asymmetric with

490 increasing kick strength, see panel (b) of Fig. X.11. For the combined interactions,
491 see panels (c) of Figs. X.10 and X.11, the carpet patterns become more complex as
492 more fractional revivals occur. However, with increasing kick strengths, the patterns
493 simplify again, exhibiting *canals* and *ridges* as well as wavepacket *focusing* (near $\theta=$
494 0) and *reversed focusing* (near $\theta=\pi$). Either is a manifestation of the *quantum-*
495 *classical correspondence* – at low kick strengths the behavior is quantum, at high
496 kick strengths quasi-classical – as a result of which the quantum carpets can in fact
497 be fitted by classical trajectories $\theta=\theta(\tau)$ at high kick strengths. The quantum-
498 classical correspondence is also apparent in the case of the pure interactions,
499 especially the orienting one, cf. Figs. X.10 and X.11.

500

501 Closely connected with the recurring patterns of the rotational wavepacket are the
502 revivals of the corresponding directional properties – orientation and alignment. As
503 the quantum carpets indicate, these happen after the kick, when the molecule is
504 field-free. The revivals occur for as long as the coherence of the rotational
505 wavepacket is maintained. A collision with another molecule or the wall of the
506 vacuum chamber upends the coherence and puts a stop to the revivals.

507

508 We note that the orientation cosine is an odd function with respect to $\tau=\pi/2$, which
509 implies that the time-averaged orientation over a full revival time τ_{rev} vanishes. In
510 contrast, the time-dependent part of the alignment cosine is an even function with
511 respect to $\pi/2$ but an odd function with respect to the quarter- and three-quarter-
512 revival times $\pi/4$ and $3\pi/4$, respectively.

513

514 Combined orienting and aligning kicks of equal strength render the molecule right-
515 way oriented for over half of the revival period. However, over the rest of the revival
516 period, when the molecule is wrong-way oriented, the orientation cosine becomes
517 greater in absolute value, however over a time interval that decreases with
518 increasing kick strength. The alignment cosine vacillates between a maximum and
519 an isotropic value (i.e., 1/3) over time intervals that are reduced at increasing kick
520 strengths.

521 [Insert Figure X.11 here]

522

523 **X.6 A Case in Point: Two Different Molecules at Various Field Combinations**

524 Let us consider two molecules from the opposite ends of Table X.1, namely DCl and
525 HXeI, for various combinations of the strengths of the electrostatic field F_1 and the
526 optical field F_2, as well as for a unipolar pulse whose strength F corresponds to that
527 of the optical field, $F = F_2$. It is instructive to see what values of the orienting and
528 aligning parameters these field combinations give rise to and what effect these, in
529 turn, have on the orientation and alignment cosines. Note that in the case of the
530 combination of an electrostatic field F_1 with an optical field F_2, only F_1 contributes to
531 the orienting parameter, whereas both F_1 and F_2 contribute to the aligning
532 parameter. This is because the effect of the optical field on the permanent dipole
533 averages out over the field's oscillating period.

534

Table X.3 summarizes the results. For DCl, one can see that in the combined electrostatic and optical fields, the interaction parameters remain quite small for F_1 ranging between 1 and 10 kV/cm and S (that gives rise to F_2) between 10^{10} and 10^{12} W/cm^2. This is mainly because of the large value of the rotational constant of DCl. The orientation and alignment cosines remain correspondingly small, but not negligible, especially at the high end of the range considered. The handicap of a large rotational constant can be completely overcome by employing a unipolar pulse of strength $F = F_2$. Although the aligning parameter remains small, the orienting parameter increases by several orders of magnitude (by a factor of 10^4 in our example), resulting in a high degree of both orientation and alignment (one can see that where there is orientation there is also alignment, but not the other way around). However, the interaction with a unipolar pulse is inherently non-adiabatic, cf. Section X.4, and the peak values of the orientation/alignment cosines attained during the rotational wavepacket revivals are only about 3/4 of the adiabatic values given in Table X.3.

The other molecular example listed in Table X.3, HXeI, is particularly amenable to orientation and alignment, even at weak combined fields. It is the compounded effect of a large permanent electric dipole moment with a large polarizability anisotropy and a small rotational constant that boosts both η and ζ and results in a pronounced directionality of the molecule. In this case, the improvement of the adiabatic values achieved by employing a unipolar pulse is only marginal.

	DCl		HXeI	
	F_1= 1 kV/cm S=10^{10} W/cm^2	F=1.948x10^3 kV/cm	F_1= 1 kV/cm S=10^{10} W/cm^2	F=1.948x10^3 kV/cm
η	0.0036	7.067	3.982	7730
ζ	0.0140	0.014	13.25	13.24
$\langle\cos\theta\rangle$	0.0012	0.732	0.851	0.9919
$\langle\cos^2\theta\rangle$	0.3338	0.598	0.747	0.9841
	F_1= 10 kV/cm S=10^{12} W/cm^2	F=1.948x10^4 kV/cm	F_1= 10 kV/cm S=10^{12} W/cm^2	F=1.948x10^4 kV/cm
η	0.0364	70.67	39.82	77295
ζ	1.430	1.424	1325	1324
$\langle\cos\theta\rangle$	0.0168	0.917	0.986	0.998
$\langle\cos^2\theta\rangle$	0.3785	0.848	0.973	0.995

Table X.3: Interaction parameters and adiabatic directional properties of DCl and HXeI molecules in their electronic, vibrational and, initially, rotational ground state $|J=0,M=0\rangle$ at choice strengths of the electrostatic field F_1 and optical field F_2 corresponding to intensity S, see Section X.2. The strength F of the unipolar field is chosen such that $F=F_2$. See also Table X.2 and text.

In a thermal ensemble of molecules characterized by a certain rotational temperature, T_r, the population of the initial rotational states will have a large effect on the directional properties of the ensemble.[71] For linear molecules, the most probable initial rotational quantum number, J^*, scales as

$$J^* \approx \left(\frac{k_B T_r}{B} \right)^{1/2}$$

where k_B is Boltzmann's constant. Since the states most amenable to orientation and alignment have the lowest initial J's, this means that a large rotational constant B, pernicious to achieving large η and ζ, will secure relatively large population of such states at a given T_r.

At a rotational temperature of 10 K, the most probable rotational state of DCl will have $J^*\approx1$, for HXeI $J^*\approx11$. At T_r=1 K, it is $J^*\approx0$ for DCl and $J^*\approx4$ for HXeI. In a ^{4}He superfluid droplet, T_r=0.38 K and $J^*\approx0$ for DCl and $J^*\approx2$ for HXeI. Thus rotational cooling and high directionality go hand in hand with one another.

X.7 Conclusions

Molecules enhanced by external electromagnetic fields gain new capacities[72]. These derive chiefly from the molecules' directional properties endowed by the fields[73]. Combined orienting and aligning fields serve to enhance these directional properties.

The principles involved in creating directional states of linear molecules by combining permanent and induced dipole forces can be generalized to symmetric[74] and asymmetric[75,76] tops. The so called 3D alignment – where all three Euler angles characterizing the rotation of an asymmetric top are aligned by an elliptically polarized optical field – could be turned into orientation by superimposing an electrostatic field. These efforts are turning molecular tomography into reality.

Manipulation of molecular translation can be achieved in inhomogeneous fields acting either on low- or high-field seekers. Molecular trapping/confinement in static fields (electric or magnetic, in case of paramagnetic molecules) is restricted to low-field seekers: this is because static fields can only have a minimum of field strength in free space (Earnshaw's theorem[29]). Despite this limitation, manipulating trajectories of low-field seekers has flourished, with prominent applications such as Stark deceleration and focusing[77], the molecular fountain[78], or the molecular synchrotron[79]. In contrast, high-field seekers can be trapped by optical fields, whose electric vector is oscillating (time dependent) and, therefore, can have a maximum of field strength in free space. Such a maximum can be achieved by focusing the electromagnetic field produced by a laser. This is the basis of "optical tweezers," i.e., a maximum of field strength at the focus of an optical field that is used to trap or seize a molecule or a functional group.[80,81] A molecule held by optical tweezers is aligned and, if its symmetry allows it, can be 3D aligned[18] as well as oriented by superimposing an electrostatic field.[82] This may be of advantage for applications in stereochemistry.

An array of counter-propagating laser beams can be used to generate an optical lattice whose lattice points/nodes can be loaded with molecules. The oriented states of the trapped molecules can serve as quantum bits (qubits). The conditions for a proper operation of quantum logic gates based on such qubits and controlled by microwave or optical pulses have already been established.[50-52,83].

Molecules in combined fields will likely continue popping up in additional applications – whether in physics, chemistry or even biology.

Acknowledgments

The work on molecules in combined fields outlined herein resulted from the combined effort of, in alphabetical order, Simon Becker (University of Cambridge), Long Cai (Caltech), Marko Härtelt (Frauenhofer Institute Freiburg), Dudley Herschbach (Harvard University), Sabre Kais (Purdue University), Mallikarjun Karra (Fritz Haber Institute), Mikhail Lemeshko (IST Austria), Lutz Martenskoetter, Marjan Mirahmadi (Freie Universität Berlin), Konrad Schatz (Society for the Advancement of Applied Computer Science, Berlin), Burkhard Schmidt (Freie Universität Berlin), Alkwin Slenczka (University of Regensburg) and Ketan Sharma (Ohio State University). I thank them all for their parts in our joint enterprise. I also thank to Henrik Stapelfeldt (University of Aarhus) for a critical reading of the manuscript and to Gerard Meijer (Fritz Haber Institute) for his continued support.

This chapter is dedicated – with much gratitude – to Dudley Herschbach.

Figures

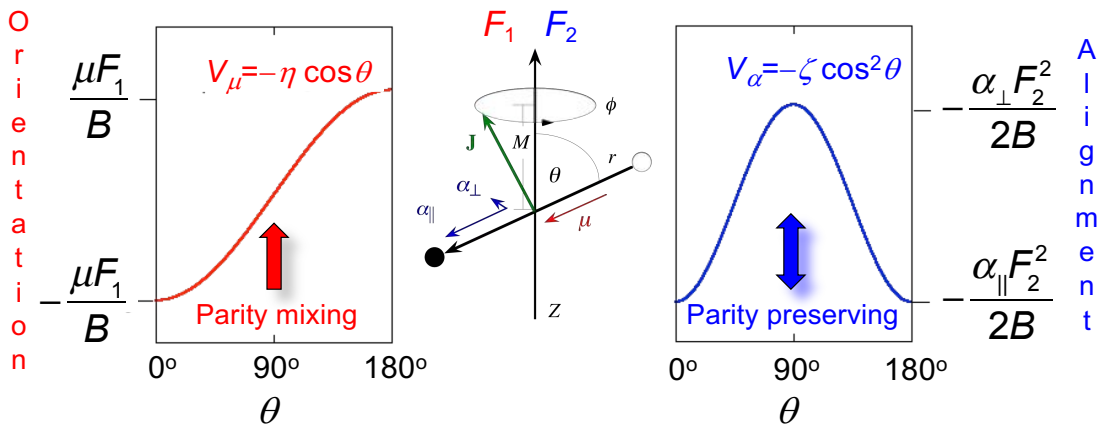

*Fig. X.1: Permanent dipole/orienting potential (on the left, in red) and induced dipole/aligning potential (on the right, in blue) as functions of the polar angle θ between the dipoles fixed to the internuclear axis r and the collinear field vectors F_1 and F_2 whose common direction defines the space-fixed Z axis. Note the cylindrical symmetry of the problem with respect to Z, which implies a uniform distribution of the azimuthal angle ϕ and a well-defined projection M on Z of the angular momentum **J**.*

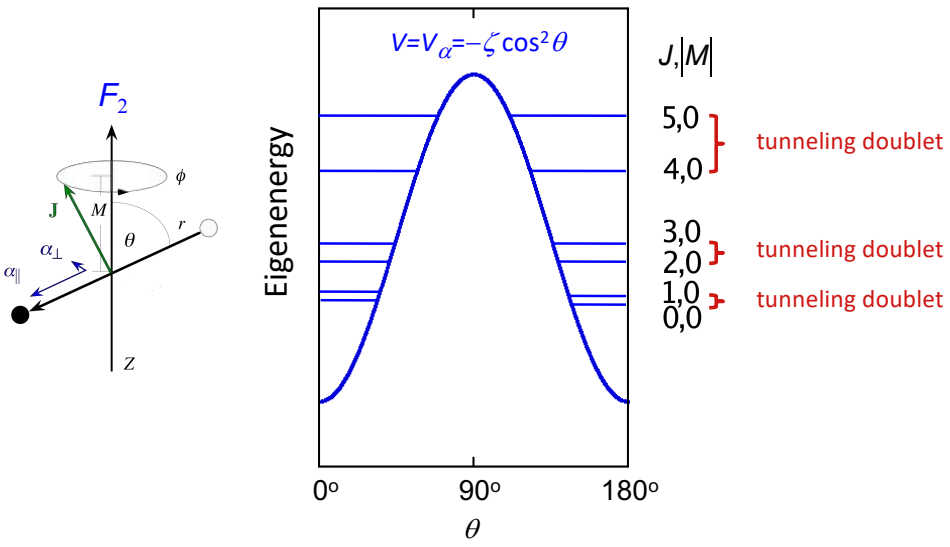

Fig. X.2: On the left is a schematic of a linear polarisable molecule subject to an an electric field. On the right is the induced dipole potential as a function of the polar angle θ between the molecular axis r and the direction of the field. Also shown are the tunnelling doublets with M = 0 that are bound by the induced dipole potential. Note the decreasing tunnelling splitting of the doublets that are bound more deeply by the potential.

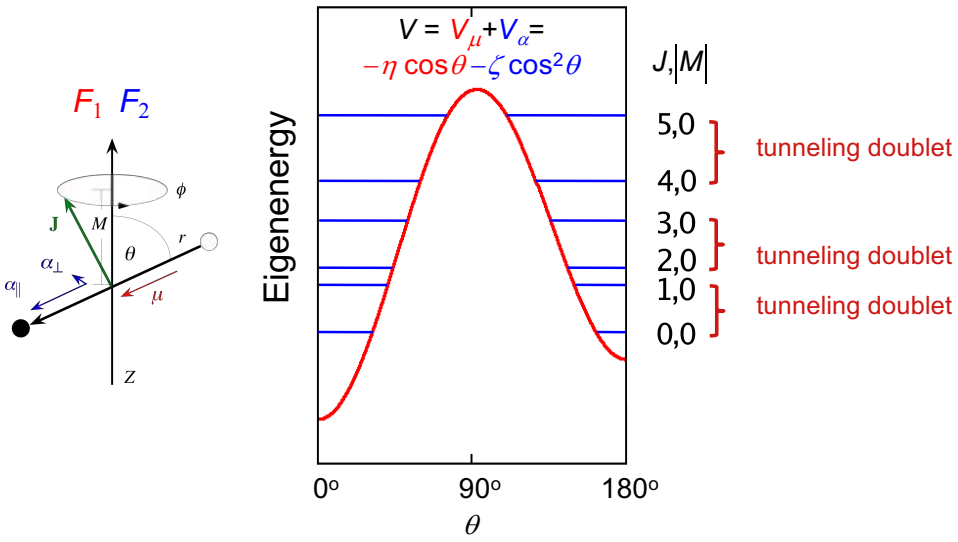

Fig. X.3: On the left is a schematic of a linear polar and polarisable molecule subject to collinear combined fields. On the right is the combined permanent and induced dipole potential as a function of the polar angle θ between the molecular axis r and the common direction of the collinear fields. Also shown are the tunnelling doublets with M = 0 that are bound by the combined potential. Note the increased splitting of the tunnelling doublets that are bound more deeply by the combined potential. See also Fig. X.2.

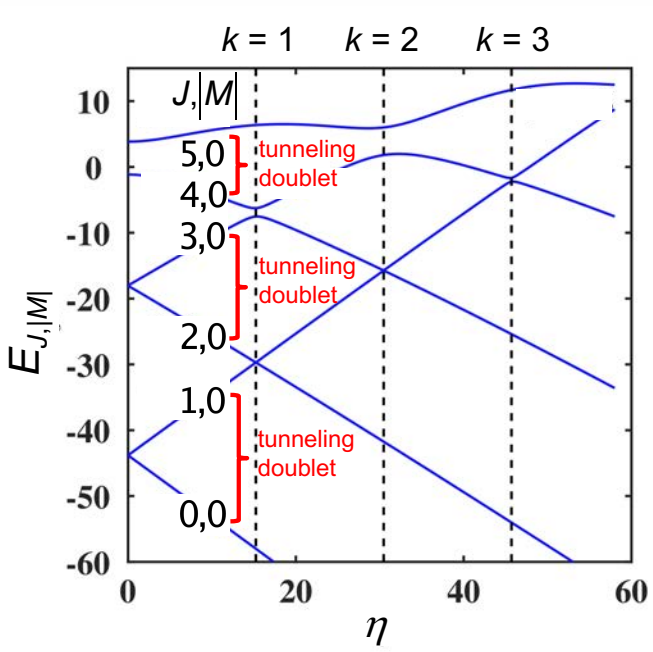

Fig. X.4: Eigenenergies of the lowest tunnelling doublets with M = 0 as functions of the orienting parameter η at a fixed values of the aligning parameter ζ = 58. The tunnelling splitting at η = 0 increases with initial J. All intersections are avoided, due to the coupling by the permanent dipole interaction of the members of different tunnelling doublets. Each state $|J,|M|;\eta,\zeta>$ undergoes J intersections. The avoided intersections are labelled by the topological index k. Note that the eigenergeies are given in terms of the rotational constant B, cf. TableX.2.See text.

699

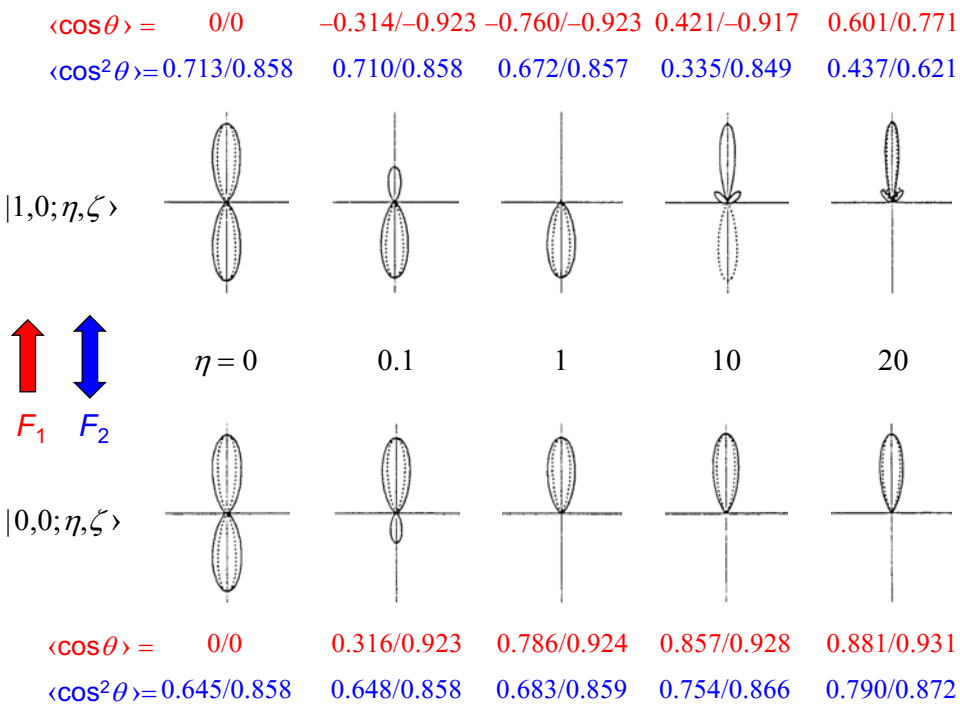

700

701 *Fig. X.5: Polar plots of the squares of the wavefunctions of Eq. (9) pertaining to the*
702 *0,0-1,0 tunnelling doublet for increasing values of the orienting parameter η and for*
703 *fixed values of the aligning parameter ζ (full curves, ζ = 10; dotted curves, ζ = 50).*
704 *Also shown are the values of the orientation (in red) and alignment (in blue) cosines*
705 *pertaining to the wavefunctions (with the value pertaining to ζ = 10 given before the*
706 *slash and the value pertaining to ζ = 50 after the slash. The arrows show the*
707 *directions of the orienting (F_1) and aligning fields (F_2). Note that the right- and wrong-*
708 *way oriented states have positive and negative values of the orientation cosine,*
709 *respectively.*

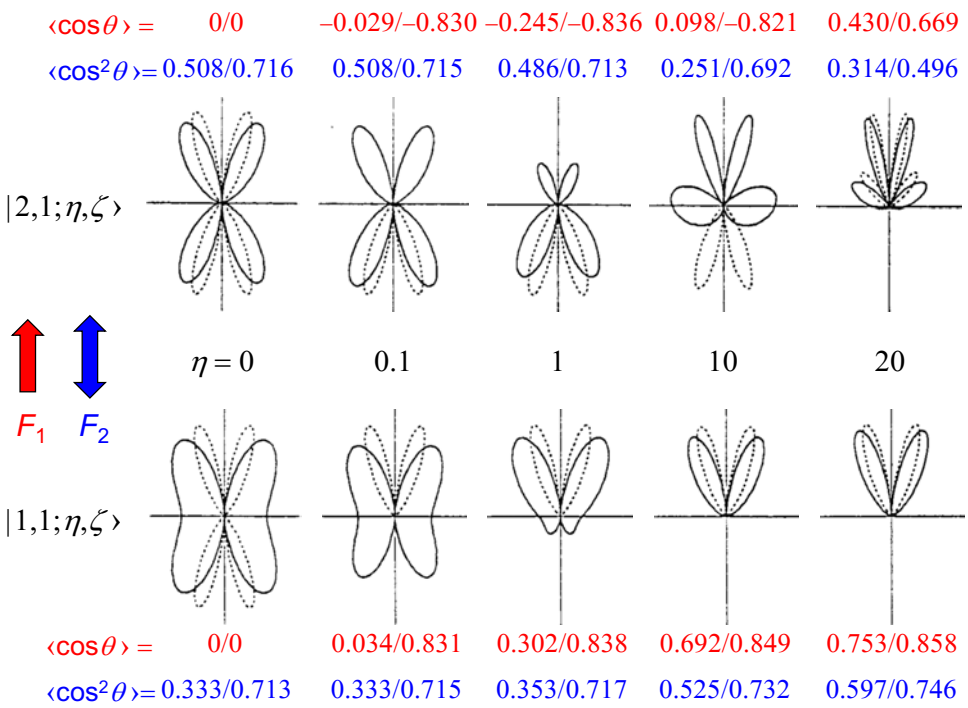

Fig. X.6: Same is in Fig. X.5 but pertaining to the 1,1-2,1 tunnelling doublet.

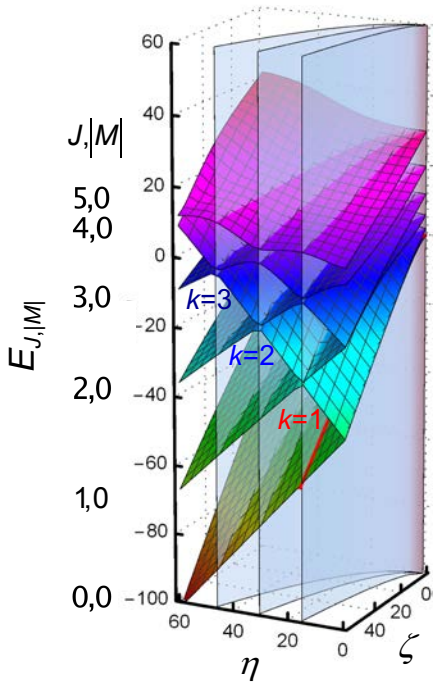

Fig. X.7: Eigenenergy surfaces of a linear polar and polarisable rotor spanned by the dimensionless orienting (η) and aligning (ζ) parameters. All surfaces shown pertain to the angular momentum projection quantum number M = 0. The avoided intersections are labelled by the topological index k. The red curve at the intersection of the ground-state surface (with J = 0) and the parabolic surface for k = 1 is an analytic eigenenergy.

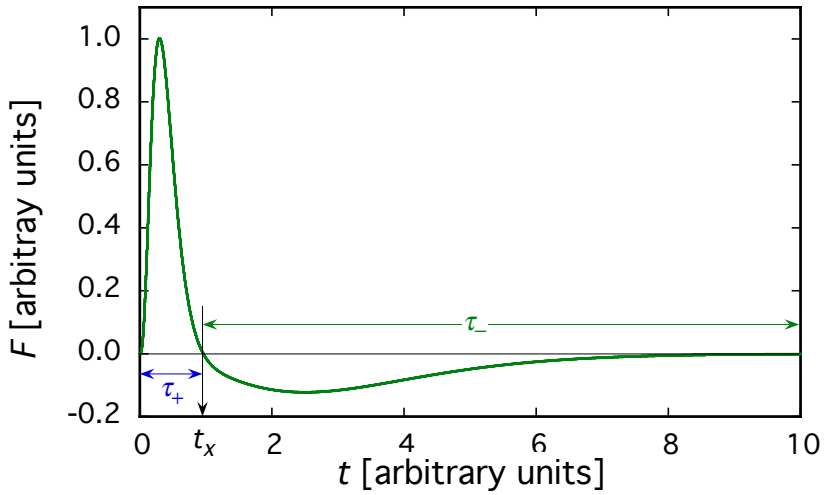

Fig. X.8: A "unipolar" electromagnetic pulse. Apart from its larger amplitude of the positive branch than in the negative one, the field $F = F_1 = F_2$ has also a different temporal dependence over the two branches. Note that the surface areas under the positive and above the negative branch of the pulse are equal.

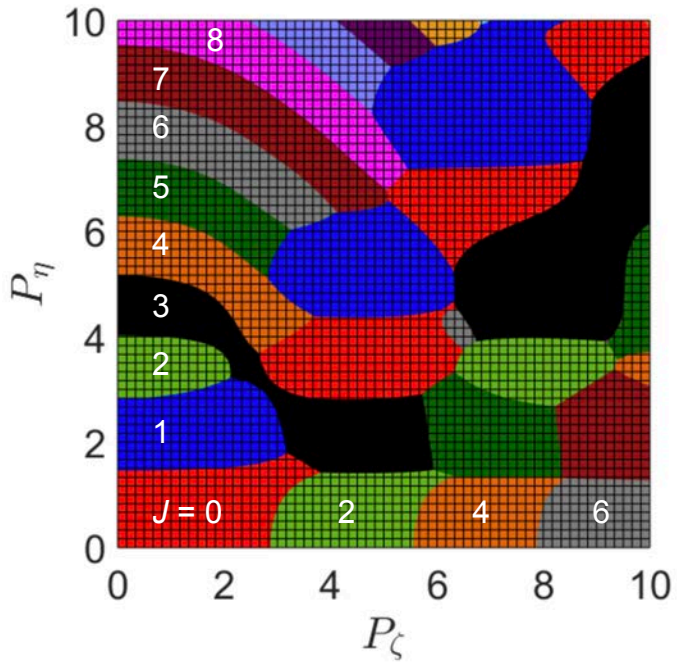

Fig. X.9: Population quilt, i.e., a top view (projection onto the P_η, P_ζ plane) of the populations of the rotational states J excited by the interaction of a molecule in the ground rotational state (J = 0) with a delta-kick. See text. Adapted from Ref.[11]

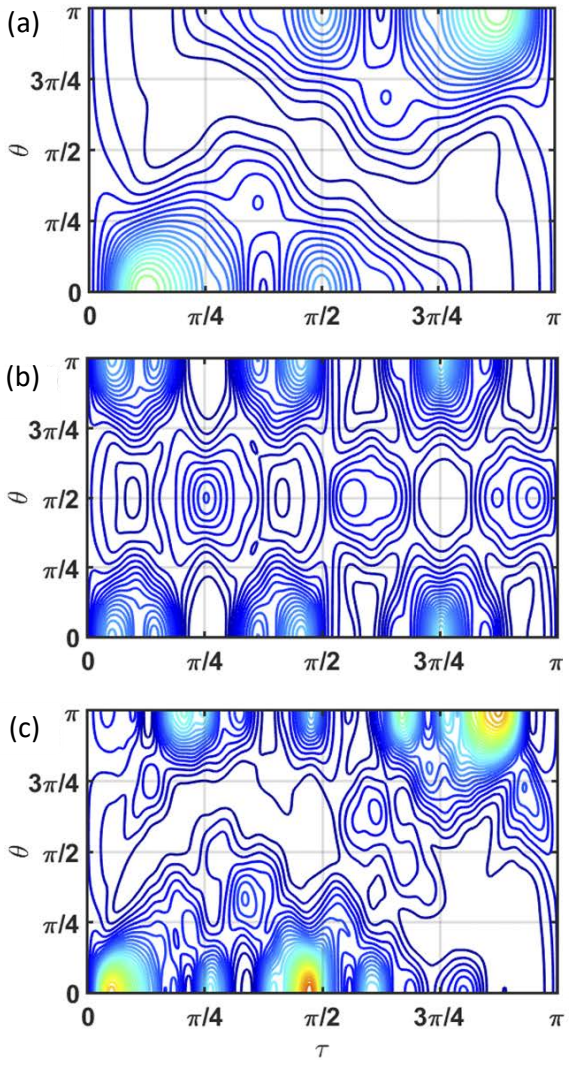

Fig. X.10: Quantum carpets, i.e., the probability densities of the polar angle θ as functions of the reduced time τ, for delta kicks of strengths P_η =1.5, P_ζ = 0 (panel a), P_η = 0, P_ζ = 1.5 (panel b), and P_η =1.5, P_ζ = 1.5 (panel c). See text. Adapted from Ref.[11]

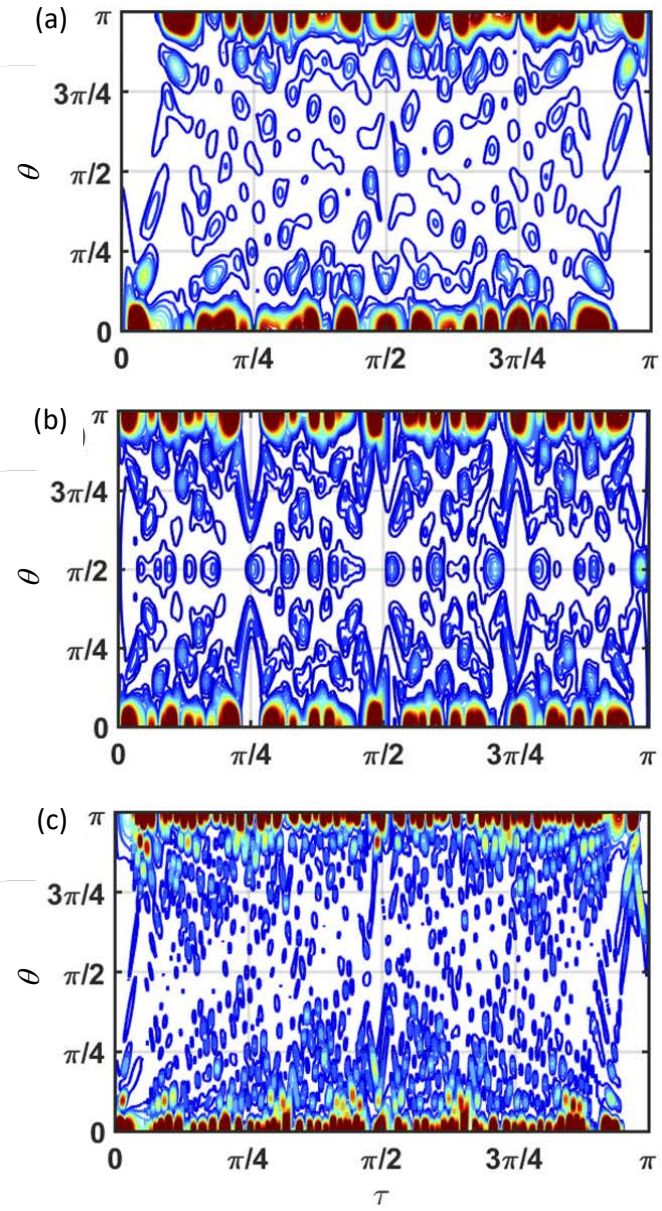

Fig. X.11: Quantum carpets for delta kicks of strengths P_η =8, P_ζ = 0 (panel a), P_η = 0, P_ζ = 8 (panel b), and P_η = 8, P_ζ = 8 (panel c). See also caption to Fig. X.10 and text. Adapted from Ref.[11]

778 **References**

[1] B. Friedrich and D. Herschbach, *The Journal of Chemical Physics*, 1999, **111**, 6157.

[2] L. Cai, J. Marango and B. Friedrich, *Physical Review Letters*, 2001, **86**, 775.

[3] H. Sakai, S. Minemoto, H. Nanjo, H. Tanji and T. Suzuki, *Physical Review Letters*, 2003, **90**, 083001.

[4] B. Friedrich, N. H. Nahler, and U. Buck, *Journal of Modern Optics*, 2003, **50**, 2677.

[5] L. Holmegaard, J. H. Nielsen, I. Nevo, H. Stapelfeldt, F. Filsinger, J. Küpper and G. Meijer, *Physical Review Letters*, 2009, **102**, 023001.

[6] J. H. Nielsen, H. Stapelfeldt, J. Küpper, B. Friedrich, J. J. Omiste and R. González-Férez, *Physical Review Letters*, 2012, **108**, 193001.

[7] B. Schmidt and B. Friedrich, *The Journal of Chemical Physics*, 2014, **140**, 064317.

[8] B. Schmidt and B. Friedrich, *Frontiers of Physics*, 2014, **2**, 1.

[9] B. Schmidt and B. Friedrich, *Physical Review A*, 2015, **91**, 022111.

[10] K. Schatz, B. Friedrich, S. Becker and B. Schmidt, *Physical Review A*, 2018, **97**, 053417.

[11] M. Mirahmadi, B. Schmidt, M. Karra and B. Friedrich, *The Journal of Chemical Physics*, 2018, **149**, 174109.

[12] L. Xu, I. Tutunnikov, E. Gershnabel, Y. Prior, and I. Sh. Averbukh, 2020, arXiv:2003.01482v1.

[13] P. Brooks, *Science*, 1976, **193**, 11.

[14] H. J. Loesch and A. Remscheid, *The Journal of Chemical Physics*, 1990, **93**, 4779.

[15] B. Friedrich and D. Herschbach, *Nature* (London), 1991, **353**, 412.

[16] J. Ortigoso, M. Rodríguez, M. Gupta and B. Friedrich, *The Journal of Chemical Physics*, 1999, **110**, 3870.

[17] T. Seideman, *Physical Review Letters*, 1999, **83**, 4971.

[18] J. J. Larsen, K. Hald, N. Bjerre, H. Stapelfeldt and T. Seideman, *Physical Review Letters*, 2000, **85**, 2470.

[19] L. Cai and B. Friedrich, *Collection of Czech Chemical Communications*, 2001, **66**, 991.

[20] I. S. Averbukh and R. Arvieu, *Physical Review Letters*, 2001, **87**, 163601.

[21] M. Leibscher, I. S. Averbukh, and H. Rabitz, *Physical Review Letters*, 2003, **90**, 213001.

[22] M. Leibscher, I. S. Averbukh, and H. Rabitz, *Physical Review A*, 2004, **69**, 013402.

[23] J. Toennies, *Zeitschrift für Physik*, 1964, **177**, 84.

[24] S. Stolte, *Berichte der Bunsen Gesellschaft für Physikalische Chemie*, 1982, **413**, 84.

[25] H. Stapelfeldt, H. Sakai, E. Constant and P. Corkum, *Physical Review Letters*, 1997, **79**, 2787.

[26] L. Y. Kim, J. H. Lee, H. A. Kim, S. K. Kwak, B. Friedrich, and B. S. Zhao, *Physical Review A*, 2016, **94**, 013428.

[27] S. Truppe, H. Williams, M. Hambach, L. Caldwell, N. Fitch, E. Hinds, B. Sauer, and M. Tarbutt, *Nature Physics*, 2017, **13**, 1173.

[28] R. Bernstein, D. Herschbach, and R. Levine*, Journal of Physical Chemistry*, 1987, **91**, 5365.

[29] R. Krems, W. C. Stwalley and B. Friedrich, *Cold Molecules: Theory, Experiment, Applications,* CRC, Boca Raton, FL, 2009.

[30] O. Dulieu and A. Osterwalder, *Cold Chemistry: Molecular Scattering and Reactivity Near Absolute Zero*, Royal Society of Chemistry, Cambridge, 2018.

[31] A. Slenczka, *Chemistry – A European Journal*, 1999, **5**, 1136.

[32] Y. Park, Hani Kang, R.W. Field and Heon Kang, *Proceedings of the National Academy of Sciences*, 2019, **116**, 23444.

[33] C. Z. Bisgaard, O. J. Clarkin, G. Wu, A. M. D. Lee, O. Gessner, C. C. Hayden and A. Stolow, *Science*, 2009, **323**, 1464.

[34] L. Holmegaard, J.L. Hansen, L. Kalhøj, S.L. Kragh, H. Stapelfeldt, F. Filsinger, J. Küpper, G. Meijer, D. Dimitrovski, M. Abu-samha, C. P. J. Martiny and L. Bojer Madsen, *Nature Physics*, 2010, **6**, 428.

[35] J. L. Hansen, H. Stapelfeldt, D. Dimitrovski, M. Abu-samha, C. P. J. Martiny and L. B. Madsen, *Physical Review Letters*, 2011, **106**, 073001.

[36] A. Landers, T. Weber, I. Ali, A. Cassimi, M. Hattass, O. Jagutzki, A. Nauert, T. Osipov, A. Staudte, M. H. Prior, H. Schmidt-Böcking, C. L. Cocke and R. Dörner, *Physical Review Letters*, 2001, **87**, 013002.

[37] R. Boll, D. Anielski, C. Bostedt, J. D. Bozek, L. Christensen, R. Coffee, S. De, P. Decleva, S. W. Epp, B. Erk, L. Foucar, F. Krasniqi, J. Küpper, A. Rouzée, B. Rudek, A. Rudenko, S. Schorb, H. Stapelfeldt, M. Stener, S. Stern, S. Techert, S. Trippel, M. J. J. Vrakking, J. Ullrich and D. Rolles, *Physical Review A*, 2013, **88**, 061402(R).

[38] J. Itatani, J. Levesque, D. Zeidler, H. Niikura, H. Pépin, J. C. Kieffer, P. B. Corkum and D. M. Villeneuve, *Nature* (London), 2004, **432**, 867.

[39] C. Jin, J. B. Bertrand, R. R. Lucchese, H. J. Wörner, P. B. Corkum, D. M. Villeneuve, A.-T. Le and C. D. Lin, *Physical Review A*, 2012, **85**, 013405.

[40] K.-J. Yuan and A. D. Bandrauk, *Physical Review A*, 2009, **80**, 053404.

[41] O. Smirnova, Y. Mairesse, S. Patchkovskii, N. Dudovich, D. Villeneuve, P. Corkum, and M. Y. Ivanov, *Nature* (London), 2009, **460**, 972.

[42] A. Rupenyan, J. B. Bertrand, D. M. Villeneuve and H. J. Wörner, *Physical Review Letters*, 2012, **108**, 033903.

[43] P.M. Kraus, B. Mignolet, D. Baykusheva, A. Rupenyan, L. Horny, E.F. Penka, G. Grassi, O. I. Tolstikhin, J. Schneider, F. Jensen, L. B. Madsen, A. D. Bandrauk, F. Remacle and H. J. Wörner, *Science*, 2015, **350**, 790.

[44] M. A. Baranov, M. Dalmonte, G. Pupillo and P. Zoller, *Chemical Reviews*, 2012, **112**, 5012.

[45] S. R. Manmana, E. M. Stoudenmire, K. R. A. Hazzard, A. M. Rey and A. V. Gorshkov, *Physical Review B*, 2013, **87**, 081106(R).

[46] D. DeMille, Physical Review Letters, 2002, 88, 067901.

[47] B. Schneider, C. Gollub, K.-L. Kompa and R. de Vivie-Riedle, *Chemical Physics*, 2007, **338**, 291.

[48] B. M. R. Korff, U. Troppmann, K.-L. Kompa and R. de Vivie-Riedle, *The Journal of Chemical Physics*, 2005, **123**, 244509.

[49] U. Troppmann, C. M. Tesch and R. de Vivie-Riedle, *Chemical Physics Letters*, 2003, **378**, 273.

[50] Q. Wei, S. Kais, B. Friedrich, and D. Herschbach, *The Journal of Chemical Physics*, 2011, **134**, 124107.

[51] Q. Wei, S. Kais, B. Friedrich, and D. Herschbach, *The Journal of Chemical Physics*, 2011, **135**, 154102.

[52] M. Karra, K. Sharma, B. Friedrich, S. Kais, and D. Herschbach, *The Journal of Chemical Physics*, 2016, **144**, 094301.

[53] P. Hockett, C.Z. Bisgaard, O.J. Clarkin and A. Stolow, *Nature Physics*, 2011, **7**, 612.

[54] L. Christensen, J.H. Nielsen, Ch.B. Brandt, Ch.B. Madsen, L.B. Madsen, C.S. Slater, A. Lauer, M. Brouard, M.P. Johansson, B. Shepperson and H. Stapelfeldt, *Physical Review Letters*, 2014, **113**, 073005.

[55] E.T. Karamatskos, S. Raabe, T. Mullins, A. Trabattoni, P. Stammer, G. Goldsztejn, R.R. Johansen, K. Długołecki, H. Stapelfeldt, M.J.J. Vrakking, S. Trippel, A. Rouzée and J. Küpper, *Nature Communications*, 2019, **10**, 3364.

[56] D. Pentlehner, J.H. Nielsen, A. Slenczka, K. Mølmer and H. Stapelfeldt, *Physical Review Letters*, 2013, **110**, 093002.

[57] B. Shepperson, A.S. Chatterley, A.A. Søndergaard, L. Christiansen, M. Lemeshko and H. Stapelfeldt, *The Journal of Chemical Physics*, 2017, **147**, 013946.

[58] B. Shepperson, A.A. Søndergaard, L. Christiansen, J. Kaczmarczyk, R.E. Zillich, M. Lemeshko and H. Stapelfeldt, *Physical Review Letters*, 2017, **118**, 203203.

[59] A.S. Chatterley, C. Schouder, L. Christiansen, B. Shepperson, M. H. Rasmussen and Henrik Stapelfeldt, *Nature Communications*, 2019, **10**, 133.

[60] J. Deiglmayr, private communication, 2013.

[61] B. Friedrich and D. Herschbach, *Journal of Physical Chemistry A*, 1999, **103**, 10280.

[62] B. Friedrich, N.H. Nahler and U Buck, *Journal of Modern Optics*, 2003, **50**, 2677.

[63] N.H. Nahler, R. Baumfalk, U. Buck, Z. Bihary, R.B. Gerber and B. Friedrich, *The Journal of Chemical Physics*, 2002, **119**, 224.

[64] M. Pettersson, J. Lundell, and M. Räsänen, *European Journal of Inorganic Chemistry*, 1999, **5**, 729.

[65] M. Aymar and O. Dulieu, *The Journal of Chemical Physics*, 2005, **122**, 204302.

[66] J. Deiglmayr, M. Aymar, R. Wester, M. Weidemüller, and O. Dulieu, *The Journal of Chemical Physics*, 2008, **129**, 064309.

[67] V. Poterya, O. Votava, M. Farnik, M. Oncak, P. Slavicek, U. Buck, and B. Friedrich, *The Journal of Chemical Physics*, 2008, **128**, 104313.

[68] Th. Brupbacher and A. Bauder, *Chemical Physics Letters*, 1990, **173**, 435.

[69] M. Lemeshko, M. Mustafa, S. Kais and B. Friedrich, *Physical Review A*, 2011, **83**, 043415.

[70] M. Lemeshko, M. Mustafa, S. Kais and B. Friedrich*, New Journal of Physics*, 2011, **13**, 063036.

[71] B. Friedrich, *European Physical Journal D*, 2006, **38**, 209.

[72] B. Friedrich, D. Herschbach, S. Kais and B. Schmidt, *SciTech Europa Quarterly*, 2018, 27 www.scitecheuropa.eu

[73] M. Lemeshko, R.V. Krems, J.M. Doyle and S. Kais, *Molecular Physics*, 2013, **111**, 1648.

[74] M. Härtelt and B. Friedrich, *The Journal of Chemical Physics*, 2008, **128**, 224313.

[75] .J. Omiste and R. González-Férez, *Physical Review A*, 2016, **94**, 063408.

[76] L.V. Thesing, J. Küpper and R. González-Férez, *The Journal of Chemical Physics*, 2017, **146**, 244304.

[77] J. Küpper, F. Filsinger, G. Meijer and H. Stapelfeldt, *Manipulating the motion of complex molecules: Deflection, focusing, and deceleration of molecular beams for quantum-state and conformer-selection*. In: Methods in Physical Chemistry. R. Schäfer and P.C. Schmidt (Eds.), Wiley-VCH, Weinheim, 2012.

[78] C. Cheng, A.P.P. van der Poel, P. Jansen, M. Quintero-Pérez, T.E. Wall, W. Ubachs and H.L. Bethlem, *Physical Review Letters*, 2016, **117**, 253201.

[79] C.E. Heiner, D. Carty, G. Meijer, and H.L. Bethlem, *Nature Physics*, 2007, **3**, 115.

[80] A. Ashkin, J. M. Dziedzic, J. E. Bjorkholm and Steven Chu, *Optics Letters*, 1986, **11**, 288.

[81] B. Friedrich and D. Herschbach, *Physical Review Letters*, 1995, **74**, 4623.

[82] I. Nevo, L. Holmegaard, J.H. Nielsen, J.L. Hansen, H. Stapelfeldt, F. Filsinger, G. Meijer and J. Küpper, *Physical Chemistry and Chemical Physics*, 2009, **11**, 9912.

[83] S. Kais (ed.), *Quantum Information and Computation for Chemistry*, Advances in Chemical Physics, Wiley, 2014.